Atmos. Chem. Phys. Discuss., 15, 32561–32605, 2015
www.atmos-chem-phys-discuss.net/15/32561/2015/
doi:10.5194/acpd-15-32561-2015

Atmospheric Chemistry and Physics Discussions

Insights into a historic severe haze weather in Shanghai: synoptic situation, boundary layer and pollutants

C. Leng[1,a], J. Duan[1], C. Xu[1], H. Zhang[2], Q. Zhang[1], Y. Wang[1], X. Li[1], L. Kong[1], J. Tao[3], T. Cheng[1], R. Zhang[4], and J. Chen[1]

[1]Shanghai Key Laboratory of Atmospheric Particle Pollution and Prevention (LAP[3]), Department of environmental science and engineering, Fudan University, Shanghai 200433, China
[2]Atmospheric Environment Institute, Chinese Research Academy of Environmental Sciences, Beijing 100012, China
[3]South China Institute of Environmental Sciences, Ministry of Environmental Protection, Guangzhou 510655, China
[4]Key Laboratory of Region Climate-Environment Research for Temperate East Asia, Institute of Atmospheric Physics, Chinese Academy of Sciences, Beijing 100029, China
[a]now at: Leibniz Institute for Tropospheric Research (TROPOS), Leipzig, 04318, Germany

Received: 25 August 2015 – Accepted: 6 November 2015 – Published: 19 November 2015

Correspondence to: T. Cheng (ttcheng@fudan.edu.cn)

Published by Copernicus Publications on behalf of the European Geosciences Union.

ACPD
15, 32561–32605, 2015

Abstract

A historic winter haze weather, characterized by long duration, large scale and strong pollution intensity, occurred in the Yangtze River Delta (YRD) region of China during the time frame of 1 to 10 December 2013. This severe haze event constituted of several hazy episodes and significantly influenced air quality throughout the region, especially in urban areas. Aerosol physical, chemical and optical properties were measured in Shanghai, where the instantaneous particulate mass burden per volume (e.g. $PM_{2.5}$) exceeded 600 $\mu g\,m^{-3}$ in some time, breaking the existing historical observation records, and examined to give insights into severe haze weathers. Inorganic water-soluble ions in particles, trace gases and aerosol scattering/absorption coefficients had the same tendency to increase evidently from clear episodes to hazy episodes. A combination of various factors contributed to the formation and evolution of the severe haze, among which meteorological conditions, local anthropogenic emissions and aerosol properties played the major roles. During the haze weather, the YRD region was under the control of a high-pressure system with extremely small surface pressure gradients. The calm surface wind and subsidence airflow were responsible for decreasing planetary boundary layer (PBL) height and constructive to the build-up of air pollutants wandering inside the region, and ultimately induced the haze occurrence. Nonlinear regression analyses indicated that single water-soluble ion did not correlated with the atmospheric visibility degradation so strong, while high ambient relative humidity (RH) indeed exerted a great impact with a correlation coefficient (R^2) of 0.41. Moreover, the close relationship was derived between atmospheric visibility and aerosols in size of 600–1400 nm with R^2 of 0.70, which further improved to 0.73 when combined aerosol hygroscopicity. This study may provide supports for the public and authorities to recognize severe haze weathers in urban environments, and act as a reference for forecasting and eliminating the occurrences of regional atmospheric pollutions in China.

ACPD
15, 32561–32605, 2015

1 Introduction

Atmospheric aerosols, either emitted from human activities and natural sources or formed by a variety of precursor photochemical reactions, exert great impacts on the earth's radiation balance and climate via directly scattering and absorbing solar and terrestrial lights, and indirectly modifying cloud and precipitation by acting as cloud condensation nuclei (CCN) (Ramanathan et al., 2001; Andreae et al., 2005; Lohmann et al., 2005). In low atmospheric layers, aerosol particles can aggregate and result in air pollutions under unfavorable diffusion conditions, and then produce the adverse effects on human health and atmospheric visibility (Wu et al., 2005). Haze is in nature the air pollution caused by fine particles, an atmospheric phenomenon that the sky clarity is obscured by dust, smoke and other dry particles, during which atmospheric visibility and relative humidity (RH) are usually below 10 km and 80 %, respectively (Wu et al., 2006; Xiao et al., 2006; Fu et al., 2008; Bell et al., 2011).

Since World War II, haze has occurred in London and Los Angeles due to the very fast economic development in those areas (McNulty, 1968; Lee, 1983; Schichtel et al., 2001). After that, the regions affected by haze have spread to North Africa, Indian Ocean and Asia etc. (Quin and Bates, 2003; Huebert er al., 2003; Du et al., 2011). Until now, the formation and evolution of haze has not been fully understood despite of many experiments carried out throughout the world, making it difficult for the governments to take effective measures to reduce the occurrence of air pollutions (Malm and Day, 2001; Huebert et al., 2003; Wu et al., 2005; Wang et al., 2006b).

China has undergone rapid economic and social development for over 30 years, which releases a large amount of anthropogenic particles and relevant precursors, and forces many cities to suffer from atmospheric pollutions. The increasing occurrences of haze or hazy days have been observed in the urban environments of northern, eastern, and southwestern China (Sun et al., 2006; Che et al., 2009). Four major regions are mostly influenced by haze in China, i.e. the Jing-Jin-Tang Region (JJT), the Yangtze River Delta (YRD), the Sichuan Base (SCB) and the Pearl River Delta (PRD). For ex-

ACPD
15, 32561–32605, 2015

ample, Liu et al. (2013) well summarized that the number of hazy days in Guangzhou (PRD) has been increasing significantly from 70 d in 2001 to 144 d in 2004, and in Beijing (JJT) decreasing quickly from 223 d in 1982 to 73 d in 2005 after a number of measures implemented on management of coal demand, motor vehicles, industrial and dust emissions. However, the haze intensity in Beijing increased once again in 2011 and posed significant effects on human society (Sun et al., 2004; Liu et al., 2013). Wang et al. (2006b) compared the chemical compositions of aerosols in dusty, hazy, and clear days in Beijing, and pointed out that $(NH_4)_2SO_4$, NH_4NO_3 and $Ca(NO_3)_2$ were the major species during hazy days in spring. By investigating the chemical characteristic of $PM_{2.5}$ and PM_{10} in Beijing, Sun et al. (2006) found that the concentrations of aerosol elements and water-soluble ions in haze-fog episodes were over 10 times higher than those in clear days. The YRD region, one of important economic core areas with large population, high urbanization and advanced industrialization in China, is facing an increase of foggy and hazy days at annual time scale recently, especially in winter (Tie and Cao, 2009). Studies of haze have become hot spots attracting more interest in the last few years. Ye et al. (2011) discovered the important role of ammonia in haze formation in Shanghai. Du et al. (2011) put insights into summertime haze events over Shanghai based on online water-soluble ionic composition of aerosols, and pointed out that the secondary pollutants resulted from significantly increasing sulfate and nitrate, which were oxidized from large amounts of anthropogenic gases of SO_2 and NO_2 in the urban atmosphere with high atmospheric oxidation ability and steady atmospheric condition. Kang et al. (2013) regarded higher accumulation mode particles and RH as the main reasons of atmospheric visibility impairment during haze based on the comprehensive analysis of a long-lasting haze episode in Nanjing.

However, available studies on haze in the YRD mainly put efforts to the chemical compositions and physical characteristics of pollutants, but in view of synoptic few focused on the entire process of haze pollutions. As a result, it would be meaningful to investigate the formation and evolution of regional haze events, and to support useful information for pollution forecast and how to reduce the incidence of regional atmo-

ACPD
15, 32561–32605, 2015

spheric pollutions. A winter haze occurred in the YRD during 1–10 December 2013, known as one historic severe pollution weather with features of long duration, large scale and strong pollution intensity. This paper performs a detailed analysis of this serious haze weather and gives insights into regional heavy atmospheric pollution in Asian fast-growing developing areas.

2 Experiment

2.1 Observation site

The measurement station was mounted on the roof of one building approximately 20 m above ground in the campus of Fudan University (31°18′ N, 121°29′ E) in Shanghai (population 24 millions), located in the east edge of the YRD region. The site is mainly surrounded by urban residential and commercial zones, approximate 40 km from the East China Sea. Asian monsoon climate dominates this region with annual man precipitation of 1119 mm mainly occurring between May and September. In addition, the wind prevails northeasterly in winter and southeasterly in summer, implying that atmospheric components are likely influenced by both local emissions and remote sources through atmospheric transportation (Du et al., 2011). Local time (LT) used in this study is eight hours ahead of UTC.

2.2 Instrument and measurements

Major water-soluble ions (Na^+, K^+, Mg^+, Ca^+, SO_4^{2-}, Cl^-, NO_3^- and NH_4^+) in ambient aerosol particles were measured by an online analyzer for Monitoring Aerosols and Gases (MARGA, ADI 2080, Netherlands) at 1 h time resolution. Ambient air is drawn into the sample box with airflow of $1\,m^3\,h^{-1}$ by air pump controlled by a mass flow controller (MFC). An internal calibration method, using bromide for the anion chromatograph and lithium for the cation chromatograph, was operated over the whole observation period to ensure the instrument to identify and measure ion species suc-

ACPD
15, 32561–32605, 2015

cessfully. Detailed information for the instructions of sampling, operation and internal calibration methods can be found elsewhere (Du et al., 2011).

Aerosol particle size distributions in 10 nm–10 µm were observed using a high-resolution wide-range particle spectrometer (WPS-1000 XP, MSP). The principle of instrument, combining laser light scattering (LPS), condensation particle counting (CPC) and differential mobility analysis (DMA), has been introduced in detail by Gao et al. (2009). DMA and CPC can effectively count particles in 10 nm–500 nm, while LPS is designed to measure particles in 350 nm–10 µm. The instrument took 3 min to scan the entire size range completely, 60 channels in DMA and 24 channels in LPS (2 s per channel). In this study, DMA was calibrated using National Institute of Standards and Technology (NIST) Standard Reference Materials (SRM) 1691 and SRM 1963 Polystyrene Latex (PSL) spheres (mean diameter of 0.269 and 0.1007 µm) to maintain DMA transferring function proper and accurate particle sizing. LPS was calculated using four NIST traceable sizes of PSL (i.e. 0.701, 1.36, 1.6 and 4.0 µm). Zhang et al. (2010) has described the calibration and operation methodology of WPS in detail.

Black carbon (BC) was measured by an online monitor of Aethalometer (AE-31, Magee Scientific Co., USA) at 5 min time resolution and 5 L min^{-1} airflow rate. According to the strong ability of BC absorption to light at near infrared wavelengths (Hansen et al., 1984; Weingartner et al., 2003), BC mass is determined using the light attenuation at 880 nm and the appropriate specific attenuation cross section proportional to BC (Petzold et al., 1997). The attenuation can be calculated based on the intensity difference of reference and sensing beams between light on and off (Dumka et al., 2010). In order to screen the impacts of other absorptive material, the data contaminated by mineral and dust aerosols were excluded from BC measurements. Details for instrument operating and calibrating can be found in Cheng et al. (2010).

Aerosol backscattering profile was measured by a set of micro pulse lidar (MPL-4B) with pulse energy 6–10 µJ and repetition frequency 2500 Hz. To date, MPL is utilized widely in the world as an effective tool for providing high temporal resolution information of aerosol vertical distributions (Menut et al., 1999; Cohn and Angevine, 2000; Brooks,

ACPD
15, 32561–32605, 2015

2003). Planetary boundary layer (PBL) height is determined by the MPL measurement at the altitude where a sudden decrease of scattering coefficients occurs (Boers and Eloranta, 1986). To avoid underestimation of aerosol scattering at the lowest altitudes with the majority of aerosol population, the overlap issue is concerned and solved experimentally (Campbell et al., 2002; He et al., 2006). In general, MPL is set horizontally to obtain an averaged atmospheric data in the late afternoon without obscuration due to relatively lower aerosol loading and well mixed atmosphere, under which condition the backscattering in the target layer is roughly assumed to constant. The calibrations operated in 2009 showed that the full overlap is about 4 km, and the raw data need to be corrected by the overlap correction function (He et al., 2006). The uncertainty induced by the overlap correction has been fully discussed and estimated to be less than 10 % (Welton et al., 2002; He et al., 2006).

Aerosol scattering coefficients (525 nm) were measured using an Aurora-1000 nephelometer (Ecotech Pty Ltd., Australia) at 5 min resolution. The scattering coefficient is calculated by integrating the scattering intensities from angles 7 to 170°. The relative humidity (RH) inside the instrument was retained below 60 % to prevent from excessive water vapor entering the chamber. By the way, the zero check was operated automatically each day using particle-free air, while the span check was done every two weeks using R-134a gas.

A CCN counter (CCN-100, DMT, USA) with continuous flow and single column (Roberts and Nenes, 2006; Lance et al., 2006) was employed to monitor CCN number concentrations at supersaturations (SS) of 0.2–1.0 %. The ambient aerosols were firstly dried by a dryer (active carbon) to lower relative humidity (RH) below 30 %, and subsequently introduced into the counter. The instrument was calibrated for SS using standard $(NH_4)_2SO_4$ particles every three months since it was mounted in the observational site in 2010. According to the instrument operation manual, regular calibrations were also performed for temperature gradient, input and shear airflows and pressure to maintain stable SS (Leng et al., 2013, 2014a, b). Periodic zero checks were done to

ACPD
15, 32561–32605, 2015

ensure counting accuracy for optical particle counter (OPC) installed inside the CCN counter.

Moreover, two continuous ambient particulate monitors (FH62C14, Thermo) were used to measure $PM_{2.5}$ and PM_{10} (particles in aerodynamic diameter $< 2.5\,\mu m$ and $< 10\,\mu m$) concentrations online. An automatic weather station (HydroMet^{TM}, Vaisala) and a visibility monitor (Vaisala) were employed to measure meteorological variables and atmospheric visibility.

3 Results and discussion

3.1 Overview of haze weather

3.1.1 Identification of hazy episode

It has been widely accepted that the key criterion for discerning a haze event is to identify an apparent decrease of atmospheric visibility less than 10 km, and ambient relative humidity (RH) below 80 % lasting for several hours (Fu et al., 2008; Du et al., 2011). When 80 % < RH < 90 %, the event is referred to as a complex of haze-fog co-occurring or transition, and it is also classified into hazy episode in the present study (Leng et al., 2014a).

Figures 1 and 2 depict the temporal variations of hourly $PM_{2.5}$, PM_{10}, atmospheric visibility and meteorological factors in Shanghai from 1 to 10 December 2013. On the whole, atmospheric visibility frequently declined to below 10 km, and RH hardly reached 90 %, mostly under 80 %, suggesting that the haze weather constituted of several individual events, namely hazy pollution episodes. The gray areas marked in Fig. 1 denoted hazy episodes, while the rest areas represented clean periods. It was clear that Shanghai suffered from most of these hazy episodes until 10 December, and subsequently loosened when atmospheric visibility improved and the clean sky took control afterwards. In fact, these hazy episodes approximately accounted for 70 %

ACPD
15, 32561–32605, 2015

of the entire observation period, with mean atmospheric visibilities of 5.65 km for the former compared to 29.45 km for the rest (30 %).

On a larger scale, this haze weather caused the historic event of severe atmospheric pollution, and attacked the most parts of central and eastern China. Also, this haze weather produced one serious problem to people's health because $PM_{2.5}$ in many cities exceeded 150 $\mu g\,m^{-3}$, and some more than 300–500 $\mu g\,m^{-3}$ even 600 $\mu g\,m^{-3}$.

3.1.2 Meteorological conditions

Precipitation did not appear during the whole campaign. For most of the measured period (Fig. 2), ambient RH and temperature correlated negatively with each other and showed an evident diurnal pattern, varying in the ranges of 20–87 % and 6–17 °C, respectively. The hazy episodes were usually characterized by higher ambient RH and lower temperature, while the clean periods often corresponded to lower RH and higher temperature. The main reason is that high temperature can strengthen the vertical dispersion of atmospheric pollutants due to thermal effects, while high RH can facilitate somewhat aerosol scattering due to hygroscopicity. The wind was weak in speed ($< 2\,m\,s^{-1}$, 87 %) during the hazy episodes until 9 December, in the following day it became strong ($> 4\,m\,s^{-1}$) and conductive to the dispersion of air pollutants due to transiting cold front (Fig. 2). The wind direction was basically northeast or southeast during the clear periods, originating from the marine areas. However, the wind normally turned into northwest when the haze took over, which will probably bring a large quantity of pollutants from the inland China and to some extent cause air pollutant accumulation in downwind areas.

3.1.3 Particulate mass concentration

$PM_{2.5}$ and PM_{10}, defined as particles with diameter less than 2.5 and 10 µm, were employed to represent ambient particulate mass burden per volume in the boundary atmosphere layer. On one hand, seen in Fig. 1, $PM_{2.5}$ and PM_{10} instantaneously ranged

ACPD
15, 32561–32605, 2015

within 50–600 and 55–680 $\mu g\,m^{-3}$ throughout the whole campaign, and both of them significantly rose during the hazy episodes with averages of 315 and 333 $\mu g\,m^{-3}$, compared to 112 and 134 $\mu g\,m^{-3}$ in the clean periods. On the other hand, the ratios of $PM_{2.5}/PM_{10}$ varied between 0.54 and 0.97, and averaged at 0.88 in total, 0.93 for the hazy episodes and 0.8 for the clean periods, indicating that $PM_{2.5}$ made a major contribution to the particle mass burden.

Interestingly, both $PM_{2.5}$ and PM_{10} reached their peaks of 600 and 680 $\mu g\,m^{-3}$ as new historic records on 6 December, approximately 19 times higher than the daily limit of USA Ambient Air Quality Standard (35 $\mu g\,m^{-3}$ for PM_{10}), 14 times higher than the Grade I criteria of the National Ambient Air Quality Standard of China (50 $\mu g\,m^{-3}$ for PM_{10}), and 24 times higher than the World Health Organization Air Quality Guidelines (25 $\mu g\,m^{-3}$ for $PM_{2.5}$). Other big cities in the YRD showed the same tendency of $PM_{2.5}$ and higher mean values over this haze weather, such as 226 $\mu g\,m^{-3}$ in Hangzhou, 230 $\mu g\,m^{-3}$ in Nanjing and 260 $\mu g\,m^{-3}$ in Hefei (Fig. 3). As Nanjing and Hefei are located at the upwind of Shanghai, the inflow of external pollutants seems inevitable. Literature database from numerous measurements performed earlier in Shanghai during the last decade showed much lower values. For example, Wang et al. (2006a) observed that $PM_{2.5}$ varied within 17.8–217.9 $\mu g\,m^{-3}$ and averaged at 94.6 $\mu g\,m^{-3}$. According to the Shanghai Environmental Bulletin 2010 (www.envir.gov.cn/law/bulletin/2010/), the annual average of PM_{10} in 2009 was about 79 $\mu g\,m^{-3}$. Leng et al. (2014a) reported $PM_{2.5}$ average of 143 $\mu g\,m^{-3}$ during hazy episode and 46 $\mu g\,m^{-3}$ during clear episode in November 2010. They also observed that $PM_{2.5}$ varied in 10–210 $\mu g\,m^{-3}$ in January 2011 and 10–130 $\mu g\,m^{-3}$ in April 2012, respectively (Leng et al., 2013, 2014b). In addition, compared to Beijing as another megacity in China, He et al. (2001), Sun et al. (2004) and Liu et al. (2013) monitored $PM_{2.5}$ extremes of 357 $\mu g\,m^{-3}$ from July 1999 to September 2000, 349 $\mu g\,m^{-3}$ in winter from 2002 to 2003, and 220 $\mu g\,m^{-3}$ in September 2011. Briefly, the particulate mass burden was extremely high in this

ACPD
15, 32561–32605, 2015

haze weather, and so serious air pollution, unsuitable for human beings (Liu et al., 2013), must cause an formidable environmental disaster.

3.1.4 Aerosol optical properties

Figure 4 shows a temporal series of BC, aerosol light scattering coefficient (Sc), and aerosol light absorption coefficient (Ab) indirectly calculated from measured BC according to the following equation, which has been described in detail by Yan et al. (2008):

$$\mathrm{Ab} = \alpha \times [\mathrm{BC}] \quad (1)$$

where [BC] represents BC mass concentration, and α is BC absorption efficiency which is adopted as 8.28 $\mathrm{m^2\,g^{-1}}$ in this paper. This value was obtained based on the intercomparison experiment performed in southern China previously, and was within the variance range of various source regions (Bergin et al., 2001; Bond and Bergstrom, 2006; Yan et al., 2009; Zhao et al., 2013). The aerosol scattering and absorption coefficients in combination determine its extinction ability, namely aerosol extinction coefficient (Ex).

$$\mathrm{Ex} = \mathrm{Ab} + \mathrm{Sc} \quad (2)$$

Basically, BC, Sc and Ab had the same tendency to increase in the hazy episodes, and reached to their max values at 00:00 LT on 6 December, i.e. 35 $\mu\mathrm{g\,m^{-3}}$, 2.8×10^3 and 290 $\mathrm{M\,m^{-1}}$, approximately 4–5 times higher than their mean values in the clean periods (8.3 $\mu\mathrm{g\,m^{-3}}$, 643 and 58 $\mathrm{M\,m^{-1}}$). The enhancement of aerosol optical properties largely contributed to atmospheric visibility decreasing, which correspondingly deteriorated to its minimum of 50 m at the same moment (Fig. 1).

3.1.5 Condensation nuclei and cloud condensation nuclei

The temporal variations of aerosol size distribution spanning from midday on 5 to 10 December were analyzed in detail to shed some light on its relationship with haze,

ACPD
15, 32561–32605, 2015

while part of measurement is not available due to instrument maintenance. Figure 5a presents a time series of aerosol size spectra and integrating particle size-resolved number concentrations (N_{CN}). N_{CN} showed an evident diurnal pattern with two peaks corresponding to the traffic rush hours, and appeared significantly higher mean and instantaneous values in the hazy episodes (15 000 and 25 000 cm^{-3}) than the clean periods (9500 and 17 000 cm^{-3}). Generally, ambient aerosol particles in higher loading mainly distributed in a wider size range over the hazy episodes than the clean periods, 20–200 nm for the former and 20–100 nm for the latter. The averaged aerosol number size distribution is shown in Fig. 5b. About 67 % of particles fell in the size range of 10–100 nm, and the percent further increased to 91 % when the size range enlarged to 10–200 nm. This result is in good agreement with the early observations that urban ambient aerosols mainly distribute in ultrafine size section (Woo et al., 2001; Gao et al., 2007), slightly higher than 62 % reported in Nanjing and 61 % in Atlanta, a little lower than 72 % in Eastern Germany and significantly lower than 94 % in Taicang (Woo et al., 2001; Tuch et al., 1997; Gao et al., 2009; Kang et al., 2013).

Cloud condensation nuclei (CCN) constitutes an important fraction of atmospheric aerosol population, and can indirectly influence global climate change through modifying the microphysical and radiative properties and lifetime of cloud (IPCC, 2013). It tends to reduce cloud droplet size and then suppress the wet precipitation in shallow and short-lived clouds (Lohmann and Feichter, 2005). To date, few attention has been paid on the impacts of haze on CCN and activated aerosol particles. Previous studies in Shanghai have found that CCN number concentration (N_{CCN}) and aerosol activity promotes effectively during the polluted periods (Leng et al., 2013, 2014). In north India, Ritesh et al. (2007) observed a significant impact of winter haze on N_{CCN}. To gather more information about CCN during haze, hourly N_{CCN} at SS of 0.2–1.0 % from midday on 5 to 10 December were plotted as a function of time in Fig. 6. Due to instrument maintenance, there are no measurements during 1–4 December. As expected, N_{CCN} increased with SS, i.e. 3800–10 000 cm^{-3} at SS 0.2 % and 4000–16 000 cm^{-3} at SS 1.0 %, and exhibited bimodal daily distributions. Agreed well with N_{CN}, N_{CCN} greatly

ACPD
15, 32561–32605, 2015

enhanced during the hazy episodes, and was about 1.6–1.8 folds (on varying SS) of that during the clean periods.

3.1.6 Aerosol chemical species

A key for understanding haze is to characterize both aerosol composition and trace gases quantitatively (Du et al., 2011). As important components of atmospheric particles, water-soluble inorganic ions are thought to be a significant contributor to atmospheric visibility impairment (Kang et al., 2013).

The time series of 1 h averaged water-soluble inorganic ions in $PM_{2.5}$, including Na^+, K^+, Mg^+, Ca^+, SO_4^{2-}, Cl^-, NO_3^- and NH_4^+, and gaseous pollutants such as SO_2, NO_2, CO and O_3 from 1 to 10 December 2013 are described in Fig. 7. Aerosol water-soluble ions highly coinciding with particulate mass burden revealed higher content in the hazy episodes than the clean periods, especially at 00:00 LT on 6 December when they were strongly enhanced almost 3 times of their averages of the clean periods. Totally, the mean concentrations of these ions were comparable to that monitored earlier in Shanghai (Yao et al., 2002; Wang et al., 2006a; Du et al., 2011). The mean concentrations of these ions were in sequence of $NO_3^- > SO_4^{2-} > NH_4^+ > Cl^- > K^+ > Na^+ > Mg^{2+}$, and their contributions to $PM_{2.5}$ were 11.7, 7.7, 6.7, 1.5, 0.6, 0.3 and 0.08 %, respectively, slightly higher than that observed in haze pollutions in Nanjing and Guangzhou (Tan et al., 2009; Kang et al., 2013). Overall, the integrated water-soluble ions accounted for 28.5 % of $PM_{2.5}$, higher than the dust event but significantly lower than the biomass burning event observed in Nanjing (Zhang et al., 2012).

Gaseous species play a vital role in atmospheric process by acting as precursors or mediums of photochemical reactions. Among them, O_3 has been widely known as the products of photochemical reactions between volatile organic compounds (VOCs) and nitrogen oxides (NO_x) with the participation of heat and sunlight, while SO_2, NO_2, and CO are mainly emitted from biomass, fuel and coal burning (Seinfeld and Pandis, 2006). Seen in Fig. 7, the measured gaseous pollutants behaved an increasing trend during the hazy episodes, with one exception of O_3 probably due to consumption by

ACPD
15, 32561–32605, 2015

oxidation of NO and other species which were largely emitted during haze (Liu et al., 2013).

NO_3^- and SO_4^{2-} are products of NO_2 and SO_2 due to atmospheric oxidation, hence their concentrations strongly depended on related gaseous precursors and oxidation rate in the atmosphere. Two equations are used to estimate the extent of this transformation process (Sun et al., 2006):

$$NOR = nNO_3^- / (nNO_3^- + nNO_2) \quad (3)$$

$$SOR = nSO_4^{2-} / (nSO_4^{2-} + nSO_2) \quad (4)$$

Where NOR and SOR means nitrogen oxidation rate and sulfur oxidation rate, *n* refers to molar concentration. It can be easily deduced that larger NOR and SOR would help to generate more atmospheric aerosols, and atmospheric photolysis reaction of SO_2 would take place if the oxidation rate exceeds 0.1 (Ohta and Okita, 1990). In the present study, NOR and SOR were always higher than 0.1 with averages of 0.14 and 0.27, respectively, suggesting that atmospheric oxidation of NO_2 and SO_2 contributed significantly to the formation of nitrate and sulfate. The average NOR was comparable to that calculated in a long-lasting haze weather in Nanjing (0.16) but apparently lower than that in Guangzhou (0.24), while the SOR was much higher that the value in Nanjing (0.13) but comparable to the value in Guangzhou (0.26) (Tan et al., 2009; Kang et al., 2013). Meanwhile, NO_2 surpassed SO_2 so strong in concentration with the mass ratio of 1.53, hence more atmospheric H_2O_2 and OH would be removed via reactions with NO_2, and the formation of SO_4^{2-} would be greatly suppressed due to the competition effect (Poppe et al., 1993). Furthermore, the mass ratio of ambient nitrate to sulfate (NO_3^-/SO_4^{2-}) can help to track the relative importance of stationary vs. mobile sources of nitrate and sulfur in the atmosphere (Yao et al., 2002). The stationary emission dominates in the sources of SO_2 and NO_2 if the ratio is less than 1.0, otherwise SO_2 and NO_2 mainly come from traffic activities (Huebert et al., 1988). Shanghai has been experiencing an increasing trend of NO_3^-/SO_4^{2-} because of the very fast development of motor vehicles over the past decade (Yao et al., 2002; Wang et al., 2006a; Fu et al.,

ACPD
15, 32561–32605, 2015

2008). Therefore, more contribution of pollutants from mobile sources is expected to the local pollutions. The mean NO_3^-/SO_4^{2-} during this haze weather was 1.53, comparable to our early measurement in 2010 (1.61), but significantly higher than those observed in haze weather in Guangzhou (1.02) and Nanjing (0.84 and 1.05) (Tan et al., 2009; Kang et al., 2013; Leng et al., 2013). The traffic-emitted SO_2 and NO_2 preponderating their stationary sources so conspicuous illustrated that the increasing traffic activities would be one of main reasons for visibility degradation in this study.

3.2 Formation and evolution of haze weather

3.2.1 Atmospheric circle and synoptic situation

During winter time, the YRD region is often influenced by clod air from north, such as cold high pressure and cold front, and surface temperature inversion takes place sometimes (Chen et al., 2003; Liu et al., 2013). Under those conditions, atmospheric mixing and dispersion are basically weak in favor of pollutant accumulation, hence haze or fog easily occurs (Xu et al., 2011; Zhao et al., 2013).

The mean geopotential height filed at 500 hPa revealed that during 1–10 December 2013 a long wave adjustment happened over the middle and high latitude of Eurasia. On 1 to 5, the atmospheric circulation in this region was representative of two troughs and one ridge, and these troughs were located in the west of the Balkhash lake and the north of Northeast China and a wide ridge of high pressure existed between them (Fig. 8). On 6, the circulation situation changed to two troughs and two ridges, and these troughs were located in the west of Lake Baikal and the east of Asia. However, over the central and southern China, there were flat westerly flows in most times with smaller radial degree and fast-moving short-wave troughs and ridges. During the haze weather, the central and southern China was mainly controlled under the stable westerly, and the YRD was affected by it. Additionally, at 700 hPa, the shear lines generated continuously and moved eastwards, and the difference between temperature and dew point mostly exceeded 4 °C, and the weak westerly and wind convergence appeared

ACPD
15, 32561–32605, 2015

over the area covered by haze clouds. At 850 hPa, the YRD was influenced by anticyclonic ring in most of time, wind speed smaller even static, and in view of temperature, this region was in one weak warm structure, isotherms relatively flat.

The surface weather maps at 06:00 (UTC) from 3–8 December are shown in Fig. 9. A slowly migrating anti-cyclone (high-pressure) overlaid the YRD region and possibly caused a build-up of pollution due to the concomitant subsidence airflow and relatively stagnant conditions. The high pressure dominating this area also indicated aloft airflow convergence and surface divergence, which would in turn subside and restrict PBL development, and accordingly limit the vertical diffusion of pollutants by trapping them within a shallow altitude. Unfavorable ambient temperature posed another adverse effect on the thermal dynamic development of PBL height. The small pressure gradients over the YRD would horizontally suppress the air circulation in large scale because of low wind speed mostly below 2 $m\,s^{-1}$ during the hazy episodes. Under those favorable situations, e.g. stable synoptic condition and calm wind, atmospheric pollutants were easily to accumulate within the surface atmospheric layer which ultimately led to severe urban air pollution. On the other hand, the YRD was sometime controlled by low pressure periphery and trough, and the pressure gradient was relatively weak. Although the low pressure was conducive to the rise of air masses, the vertical movement of upper and lower levels of the atmosphere was too weak to produce the effective dispersion of air pollutants and then result in pollution. Furthermore, the effect of ambient aerosols uptaking water vapor would effectively enhance their ability of scattering or absorbing solar radiation and damage atmospheric visibility eventually. The high ambient RH (60–80 %) over this haze process indeed made a rich supply of water vapor for enhancing aerosol hygroscopic growth potential and was mostly responsible for the atmospheric visibility impairment. Normally, external forces such as high wind or rainfall would be necessary to interrupt the stable situation and favor the diffusion of pollutants.

Over the target region (30°40′ ~ 31°53′), during the haze weather, the vertical winds almost were less than 0.4 $Pa\,s^{-1}$ between 500 hPa and surface, and it was less than 0.2 $Pa\,s^{-1}$ at 700 hPa, implying that the vertical exchange of air parcels between the

ACPD
15, 32561–32605, 2015

upper and lower atmospheric layers is very weak. Near the ground, the vertical velocity of winds was positive, and the relative vorticity was zero or negative value in most of time, demonstrating that airflow was prevailed in downdraft at the bottom of the atmosphere. Moreover, the temperature profile of sounding data revealed that the strong inversions occurred in 5 days with relatively low heights, so atmospheric convection and turbulence were inhibited, and then the blocked diffusion in vertical direction caused pollutant accumulation near the surface.

In summary, atmospheric pollutants were restricted within shallow layer wandering inside the YRD region favorable for visibility impairment due to the dominance of weak high pressure system with low pressure gradients, subsidence airflow, unfavorable PBL height and meteorological situation. In good agreement with our study, Wu et al. (2005) reported that descending air motion and weak horizontal wind produced significantly high particle concentrations via analyzing a severe haze event in Guangzhou. Also in the YRD area, Fu et al. (2008) found that high pressure system responsible for stagnant conditions was the major reason of high pollution events. The stable synoptic condition and its long duration was indeed viewed as one of the most important factors ruling the formation and evolution of this haze weather.

3.2.2 Impacts of air mass pathways

HYSPLIT-4 model, developed by the Air Resources Laboratory (ARL) of the National Oceanic and Atmospheric Administration (NOAA) of USA (Draxler and Rolph, 2003), was employed to compute 48 h air mass backward trajectories at 500 m height, starting at 00:00 and 12:00 UTC for each day. By doing so, we can identify and compile a full view of the impact of different source regions on the haze occurrence.

According to those calculated trajectories plotted in Fig. 10, three types of air mass pathways were determined in summary. Firstly, the air mass wandered inside the region with shallow atmospheric boundary layer, accounting for 60 % of total trajectories, which was in good agreement with stable synoptic condition during the hazy episodes. This situation facilitates the accumulation of atmospheric pollutants and ultimately re-

ACPD
15, 32561–32605, 2015

sults in haze formation. Secondly, the subsidence flow from high altitude with minor horizontal movement, accounting for 30 % of trajectories, dominated and brought in temporal clear sky between the hazy episodes on 2, 3 and 8 December. Thirdly, the air mass, originating from the northern inland China at high altitude, fast travelled southerly across the Northern China Plain (NCP) and the Eastern Region of China (ERC), and finally arrived in Shanghai over a long distance on 10 December, accounting for 10 % of trajectories. They are helpful to dilute the atmospheric pollutants and then end this haze event. Most possibly, a combination of local emissions and long-distance transportation of remote emissions exerts the joint effects to the pollutants during the haze weather.

3.2.3 High aerosol columnar loading

Aerosol optical depth (AOD), retrieved as daily averages from the remote sensing of MODIS employing the algorithm well introduced by Li et al. (2005), can be acted as a good indicator of aerosol loading in the whole atmosphere. Figure 11 depicts a full feature of AOD spatial distribution and its day-to-day development during the haze weather. Briefly, the covering region of high AODs (> 0.5) was generally spreading out a big domain, about most of the South China. High AODs originated from the YRD and the SCB, and then extended to the central South China, the southwestern China and even the south of the JJT region, and moving to the YRD area in the end.

In the most serious days, AODs were at levels as high as 1.00–1.25 on 5–8 December. For example, according to the records of the Ministry of Environmental Protection of China (http://www.zhb.gov.cn/), many cities in the upwind areas of Shanghai, such as Nanjing, Wuxi, and Suzhou, had higher AODs up to 1.5 and AQI over 500 implying that the inflow of particulate pollutants to Shanghai would be inevitable and contribute to the pollution occurrence. On the other hand, the weak circulation (Sect. 3.2.1) normally led to the build-up of pollutant pooling from local emissions especially traffic sources, giving another contribution to the haze weather formation.

ACPD
15, 32561–32605, 2015

3.2.4 Reduction of PBL height

PBL plays a vital role in determining the vertical dispersion of air pollutants that are emitted naturally or artificially from the Earth surface (Kim et al., 2007; Liu et al., 2013). Decreasing height of PBL can normally hold the pollutants within the shallow surface layer, suppress the vertical atmospheric dilution and ultimately cause regional environment shrouded by haze pollution (Kim et al., 2007). In Shanghai, several filed measurements have monitored that PBL height is usually low during hazy episodes (Leng et al., 2014b; Zhang et al., 2015). By utilizing the normalized Lidar backscatter signal at 532 nm, the PBL retrieval at 30 s resolution was derived in this study, and the time-height series was plotted in red line in Fig. 12. Overall, PBL height was negatively correlated with atmospheric visibility with R^2 of 0.63, and averaged at 1.3 km during the clean periods and 0.6 km during the hazy episodes. From midday on 5 to the night on 6 December, the height of PBL decreased to 400 m lasting more than 30 h, and $PM_{2.5}$ during this period enhanced to over 600 $\mu g\,m^{-3}$, 5.4 times of the average of the clear periods. The lower PBL heights will retain more pollutants in the surface layer and cause the city surrounded by haze.

In theory, PBL basically evolves as a function of atmospheric thermal and dynamic factors, e.g. air temperature and wind speed (Liu et al., 2013). In fact, there is a feedback between atmospheric aerosol loading and PBL height. Briefly, the more ambient aerosols accumulate, the less solar radiation reaches to surface, which inevitably poses a disadvantageous effect on surface air temperature as well as a positive impact on ambient RH, and further restricts the development of PBL. The low PBL height would in turn force the accumulation of aerosol particles under RH in the shallow atmosphere, and ultimately degrade atmospheric visibility (Liu et al., 2013). Otherwise, more solar radiation arrives at the ground in case of clean sky, under those conditions the air temperature and PBL height would increase while the ambient RH would drop, which is unfavorable to the haze formation. This scientific issue involves many complicated atmospheric processes remaining poorly understood as well as deserving further study.

ACPD
15, 32561–32605, 2015

As mentioned in Sects. 3.2.1 and 3.2.2, the YRD region was undergoing a large scale of weak high pressure with surface air moving slowly during the campaign. The air temperature retained at a low level which was also not so conductive to the development of PBL height, thereby heavy air pollution took place and eventually resulted in visibility degradation. In short, the low PBL height is helpful for the increasing of aerosol particles, hence favors the occurrence of haze weather.

3.2.5 Aerosol composition and hygroscopicity

As important components of ambient particles, particle-phase water-soluble inorganic ions generally account for 30 % of particulate matter in urban atmosphere, and are considered as a great contributor to the atmospheric visibility impairment because they hugely determine the ability of aerosol particles to uptake water vapor (Hillamo et al., 1998; Andrews et al., 2000; Chow et al., 2006; Seinfeld and Pandis, 2006). Also, they are essential participants in the formation, growth and evolution processes of nanoparticles because their presence in the atmosphere can provide significant potential of surface chemical reactions in aerosol particles (Wang et al., 2006b). In Shanghai, sulfate and nitrate have been evidently identified as great contributors to the occurrence of heavy particulate pollution events (Wang et al., 2006b; Sun et al., 2006; Fu et al., 2008), and NH_3 was observed to play a vital role in the enhancement of particulate sulfate and nitrate, and $(NH_4)_2SO_4$ and NH_4NO_3 provided a strong support to the haze formation (Ye et al., 2011).

When ambient RH is high, those aerosols that are more hydrophilic can grow in diameter via uptaking water vapor, and through this way they can increase their ability of scattering light and causing atmospheric visibility impairment (Tang, 1996). A kappa value κ, describing particle hygroscopicity, was firstly introduced by Petters and Kreidenweis (2007) and employed here to investigate its relationship with haze formation. Assuming ambient aerosols are well internal-mixed, the effective integrated κ can be

ACPD
15, 32561–32605, 2015

obtained through weighting their chemical compound volume fractions,

$$\kappa = \sum_i \varepsilon_i \kappa_i \quad (5)$$

where ε_i is the volume fraction of chemical compounds in particles, and κ_i is the effective κ of individual chemical composition. Equation (5) has been widely used and described elsewhere in detail (Petters and and Kreidenweis., 2008; Yue et al., 2011; Leng et al., 2014a, b). In this study, aerosol particle compositions were classified into three categories, and κ_i and ε_i for individual composition are listed in Table 1, of which "others" refers to PM_{10}-(SO_4^{2-} + NO_3^- + NH_4^+ + Cl^- + Na^+), and is viewed as a chemical compound with $\kappa_i = 0$ (Yue et al., 2011). Figure 12 provides the time series of the hourly-averaged kappa values, with higher κ during the hazy episodes (0.22) and lower κ during the clear periods (0.15) on average, indicating that aerosols are basically more hygroscopic responsible for haze occurrence during the pollution period.

With the aim of better understanding the potential contribution of individual water-soluble ions, BC and ambient RH to atmospheric visibility impairment, we run nonlinear regression analysis correlation analysis and the results were plotted in Fig. 13. The correlation between atmospheric visibility and individual ions, BC and $PM_{2.5}$ was not so impressive with R^2 from 0.11 to 0.22. However, it became more significant in view of ambient RH with R^2 of 0.41. The result suggests that the atmospheric visibility impairment is less driven by single water-soluble ions but largely induced by high ambient RH, in consistent with Tang (1996) and Roeland et al. (2014).

3.2.6 Aerosol size spectra

Atmospheric aerosol particles usually are divided into four classes according to their size distribution, i.e. nucleation mode (< 25 nm), Aitken mode (25–100 nm), accumulation mode (100–1000 nm), and coarse mode (> 1000 nm) (Zhang et al., 2010). The ability in determining the amount of visible light scattered by atmospheric aerosols relies strongly on their number size distributions, of which accumulation mode plays the

ACPD
15, 32561–32605, 2015

major role yet coarse and nucleation mode exert a minor contribution (Cheng et al., 2008b). Numerous studies have observed the inter-relationship between atmospheric visibility and aerosol number size distribution (Cheng et al., 2008; Roeland et al., 2014). To be more specific, Kang et al. (2013) reported that the expected reciprocal relationship was found only between atmospheric visibility and aerosols in 600–1400 nm instead of other sizes.

Accordingly, aerosol particles were classified into three categories, i.e. 10–600 nm, 600 nm–1.4 µm and 1.4–10 µm. By doing so, their nonlinear regression analysis with atmospheric visibility was computed and the results were given in Fig. 14. As expected, no significant correlation was derived between atmospheric visibility and aerosol size of 10–600 nm and 1.4–10 µm, whereas aerosols in 600 nm–1.4 µm indeed controlled atmospheric visibility to a great extent with R^2 of 0.70, which further improved to 0.73 if we combined aerosol hygroscopic potential well determined by its size-resolved composition. In this study, aerosol number concentrations in 600 nm–1.4 µm were on average 110 cm^{-3} during the hazy episodes and 43 cm^{-3} during the clean periods. The atmospheric visibility was so dependent on aerosol number size distribution and its impairment during the hazy episodes was mostly caused by the enhancement of aerosol concentration in 600 nm–1.4 µm.

4 Summary and conclusion

A historic haze event was fully analyzed for the temporal variations of atmospheric aerosol optical, physical and chemical properties and meteorological conditions, as well as the formation and evolution mechanism. During the event, atmospheric visibility decreased dramatically, while particulate burden, water-soluble inorganic ions, aerosol scattering and absorption coefficients having the same tendency increased evidently. In particular, particulate mass burden produced a new historic record by exceeding 600 µg m^{-3}.

ACPD
15, 32561–32605, 2015

Many factors in combination drove the formation and evolution of this severe haze event. For most of the measured period, the YRD region was under the control of a slowly migrating anti-cyclone resulting in subsidence airflow and relatively stagnant conditions. The subsidence airflow, which would restrict the PBL height, suppressed vertical mixing and favored the accumulation of air pollutants within the shallow atmospheric layer. Moreover, the calm surface wind subsidence airflow was not constructive to the horizontal dispersion of air pollutants which further promoted the haze formation. In summary, the significant increase of regional pollutants from anthropogenic emissions was the basic cause of this haze formation, and the unfavorable meteorological conditions played as the external reason.

Acknowledgements. This research is supported by the National Key Technology R&D Program of Ministry of Science and Technology (2014BAC16B01), the National Natural Science Foundation of China (41475109), and partly by the Shanghai Science and Technology Commission of Shanghai Municipality (12DJ1400100, 12DZ2260200), the Jiangsu Collaborative Innovation Center for Climate Change, and the Key Laboratory for Aerosol-Cloud-Precipitation of China Meteorological Administration (KDW1401).

References

Andrews, E., Saxena, P., Mussara, S., Hildemann, L. M., Koutrakis, P., McMurry, P. H., Olmez, I., and White, W. H.: Concentration and composition of atmospheric aerosols from the 1995 SEAVS experiment and a review of the closure between chemical and gravimetric measurements, J. Air Waste Manage. Assoc., 50, 648–664, 2000.

Bell, M. L., Cifuentes, L. A., Davis, D. L., Cushing, E., Telles, A. G., and Gouveia, N.: Environmental health indicators and a case study of air pollution in Latin American cities, Environ. Res., 111, 57–66, 2011.

Bergin, M., Cass, G. R., Xu, J., Fang, F., Zeng, L. M., Yu, T., Salmon, L. G., Kiang, C. S., Tang, X. Y., Zhang, Y. H., and Chameides, W. L.: Aerosol radiative, physical, and chemical properties in Beijing during June 1999, J. Geophys. Res., 106, 17969–17980, 2001.

ACPD
15, 32561–32605, 2015

Boers, R. and Eloranta, E. W.: Lidar measurements of the atmospheric entrainment zone and the potential temperature jump across the top of the mixed layer, Bound.-Lay. Meteorol., 34, 357–375, 1986.
Bond, T. C. and Bergstrom, R. W.: Light absorption by carbonaceous particles: an investigative review, Aerosol Sci. Tech., 40, 27–47, 2006.
Brooks, I. M.: Finding boundary layer top: application of a wavelet covariance transform to lidar backscatter profiles, J. Atmos. Ocean. Tech., 20, 1092–1105, 2003.
Campbell, J. R., Hlavka, D. L., Welton, E. J., Flynn, C. J., Turner, D. D., Spinhirne, J. D., Scott, V. S., and Hwang, I. H.: Full-time, eye-safe cloud and aerosol lidar observation at atmospheric radiation measurement program sites: instruments and data processing, J. Atmos. Ocean. Tech., 19, 431–442, 2002.
Che, H. Z., Zhang, X. Y., Li, Y., Zhou, Z. J., Qu, J. J., Hao, X. J.: Haze trends over the capital cities of 31 provinces in China, 1981–2005, Theor. Appl. Climatol., 97, 235–242, 2009.
Chen, L. W. A., Chow, J. C., Doddridge, B. G., Dickerson, R. R., Ryan, W. F., and Mueller, P. K.: Analysis of a summertime $PM_{2.5}$ and haze episode in the mid-Atlantic region, J. Air Waste Manage. Assoc., 53, 946–956, 2003.
Cheng, T. T., Han, Z. W., Zhang, R. J., Du, H. H., Jia, X., Wang, J. J., and Yao, J. Y.: Black carbon in a continental semi-arid area of Northeast China and its possible sources of fire emission, J. Geophys. Res., 115, D23204, doi:10.1029/2009JD013523, 2010.
Cheng, Y. F., Wiedensohler, A., Eichler, H., Heintzenberg, J., Tesche, M., Ansmann, A., Wendisch, M., Su, H., Althausen, D., Herrmann, H., Gnauk, T., Bruggemann, E., Hu, M., and Zhang, Y. H.: Relative humidity dependence of aerosol optical properties and direct radiative forcing in the surface boundary layer at Xinken in Pearl River Delta of China: an observation based numerical study, Atmos. Environ., 42, 6373–6397, 2008a.
Cheng, Y. F., Wiedensohler, A., Eichler, H., Su, H., Gnauk, T., Brüggemann, E., Herrmann, H., Heintzenberg, J., Slanina, J., Tuch, T., Hu, M., and Zhang, Y. H.: Aerosol optical properties and related chemical apportionment at Xinken in Pearl River Delta of China, Atmos. Environ., 42, 6351–6372, 2008b.
Chow, J. C., Chen, L. W. A., Watson, J. G., Lowenthal, D. H., Magliano, K. A., Turkiewicz, K., and Lehrman, D. E.: $PM_{2.5}$ cheimcal composition and spatiotemporal variability during the California regional $PM_{10}/PM_{2.5}$ air quality study (CRPAQS), J. Geophys. Res., 111, D10S04, doi:10.1029/2005JD006457, 2006.

ACPD
15, 32561–32605, 2015

Cohn, S. A. and Angevine, W. M.: Boundary layer height and entrainment zone thickness measured by lidars and wind-profiling radars, J. Appl. Meteorol., 39, 1233–1247, 2000.
Draxler, R. R. and Rolph, G. D.: HYSPLIT (Hybrid Single-Particle Lagrangian Integrated Trajectory) Model access via NOAA ARL READY Website, available at: http://www.arl.noaa.gov/ready/hysplit4.htm (last access: 8 August 2015), NOAA Air Resources Laboratory, Silver Spring, MD, 2003.
Du, H. H., Kong, L. D., Cheng, T. T., Chen, J. M., Du, J. F., Li, L., Xia, X. G., Leng, C. P., and Huang, G. H.: Insights into summertime haze pollution events over Shanghai based on online water-soluble ionic composition of aerosols, Atmos. Environ., 45, 51311–5137, 2011.
Dumka, U. C., Krishna Moorthy, K., Kumar, R., Hegde, P., Sagar, R., Pant, P., Singh, N., and Suresh Babu, S.: Characteristics of aerosol black carbon mass concentration over a high altitude location in the Central Himalayas from multi-year measurements, Atmos. Res., 96, 510–521, 2010.
Fu, Q. Y., Zhuang, G. S., Wang, J., Xu, C., Huang, K., Li, J., Hou, B., Lu, T., and Streets, D. G.: Mechanism of formation of the heaviest pollution episode ever recorded in the Yangtze River Delta, China, Atmos. Environ., 42, 2023–2036, 2008.
Gao, J., Wang, J., Cheng, S. H., Xue, L. K., Yan, H. Z., Hou, L. J., Jiang, Y. Q., and Wang, W. X.: Number concentration and size distributions of submicron particles in Jinan urban area: characteristics in summer and winter, J. Environ. Sci., 19, 1466–1473, 2007.
Gao, J., Wang, T., Zhou, X. H., Wu, W. S., and Wang, W. X.: Measurement of aerosol number size distributions in the Yangtze River delta in China: formation and growth of particles under polluted conditions, Atmos. Environ., 43, 829–836, 2009.
Hansen, A. D. A., Rosen, H., and Novakov, T.: The aethalometer-an instrument for the real-time measurement of optical absorption by aerosol particles, Sci. Total Environ., 36, 191–196, 1984.
He, Q. S., Li, C. C., Mao, J. T., Lau, A. K. H., and Li, P. R.: A study on the aerosol extinction-to-backscatter ratio with combination of micro-pulse LIDAR and MODIS over Hong Kong, Atmos. Chem. Phys., 6, 3243–3256, doi:10.5194/acp-6-3243-2006, 2006.
Hillamo, R., Allegrini, I., Sparapani, R., and Kerminen, V. M.: Mass size distributions and precursor gas concentrations of major inorganic ions in Antarctica aerosol, Int. J. Environ. Anal. Chem., 71, 357–369, 1998.

ACPD
15, 32561–32605, 2015

Huebert, B. J., Wang, M. X., and Lv, W. X.: Atmospheric nitrate, sulfate, ammonium and calcium concentrations in China, Tellus B, 40, 260–269, doi:10.1111/j.1600-0889.1988.tb00296.x, 1988.

Huebert, B. J., Bates, T., Russell, P. B., Shi, G. Y., Kim, Y. J., Kawamura, K., Carmichael, G., and Nakajima, T.: An overview of ACE-Asia: strategies for quantifying the relationships between Asian aerosols and their climatic impacts, J. Geophys. Res., 108, 1–20, 2003.

IPCC: Climate Change 2013: The Physical Science Basis. Contribution of Working Group I to the Fifth Assessment Report of the Intergovernmental Panel on Climate Change, edited by: Joussaume, S. Penner, J., and Tangang, F., IPCC, Stockholm, 2013.

Kang, H. Q., Zhu, B., Su, J. F., Wang, H. L., Zhang, Q. C., and Wang, F.: Analysis of a long-lasting haze episode in Nanjing, China, Atmos. Res., 120–121, 78–87, 2013.

Kim, S. W., Yoon, S. C., Won, J. G., and Choi, S. C.: Ground-based remote sensing measurements of aerosol and ozone in an urban area: a case study of mixing height evolution and its effect on ground-level ozone concentrations, Atmos. Environ., 41, 7069–7081, 2007.

Lance, S., Medina, J., Smith, J. N., and Nenes, A.: Mapping the operation of the DMT Continuous Flow CCN counter, Aerosol Sci. Tech., 40, 242–254, 2006.

Lee, D. O.: Trends in summer visibility in London and Southern England 1962–1979, Atmos. Environ., 17, 151–159, 1983.

Leng, C. P., Cheng, T. T., Chen, J. M., Zhang, R. J., Tao, J., Huang, G. H., Zha, S. P., Zhang, M. G., Fang, W., Li, X., and Li, L.: Measurements of surface cloud condensation nuclei and aerosol activity in downtown Shanghai, Atmos. Environ., 69, 354–361, 2013.

Leng, C., Zhang, Q., Zhang, D., Xu, C., Cheng, T., Zhang, R., Tao, J., Chen, J., Zha, S., Zhang, Y., Li, X., Kong, L., and Gao, W.: Variations of cloud condensation nuclei (CCN) and aerosol activity during fog–haze episode: a case study from Shanghai, Atmos. Chem. Phys., 14, 12499–12512, doi:10.5194/acp-14-12499-2014, 2014a.

Leng, C., Zhang, Q., Tao, J., Zhang, H., Zhang, D., Xu, C., Li, X., Kong, L., Cheng, T., Zhang, R., Yang, X., Chen, J., Qiao, L., Lou, S., Wang, H., and Chen, C.: Impacts of new particle formation on aerosol cloud condensation nuclei (CCN) activity in Shanghai: case study, Atmos. Chem. Phys., 14, 11353–11365, doi:10.5194/acp-14-11353-2014, 2014b.

Li, C., Lau, K. H., Mao, J., and Chu, D. A.: Retrieval, validation and application of the 1-km aerosol optical depth from MODIS measurements over Hong Kong, IEEE T. Geosci. Remote, 43, 2650–2658, 2005.

ACPD
15, 32561–32605, 2015

Liu, X. G., Li, J., Qu, Y., Han, T., Hou, L., Gu, J., Chen, C., Yang, Y., Liu, X., Yang, T., Zhang, Y., Tian, H., and Hu, M.: Formation and evolution mechanism of regional haze: a case study in the megacity Beijing, China, Atmos. Chem. Phys., 13, 4501–4514, doi:10.5194/acp-13-4501-2013, 2013.
Lohmann, U. and Feichter, J.: Global indirect aerosol effects: a review, Atmos. Chem. Phys., 5, 715–737, doi:10.5194/acp-5-715-2005, 2005.
Malm, W. C. and Day, D. E.: Estimates of aerosol species scattering characteristics as a function of relative humidity, Atmos. Environ., 35, 2845–02860, 2001.
McNulty, R. P.: The effect of air pollutants on visibility in fog and haze at New York city, Atmos. Environ., 2, 625–628, 1968.
Menut, L., Flamant, C., Pelon, J., and Flamant, P. H.: Urban boundary-layer height determination from lidar measurements over the Paris area, Appl. Optics, 38, 945–954, 1999.
Ohta, S., Okita, T.: A chemical characterization of atmospheric aerosol in Sapporo, Atmos. Environ., 24A, 815–822, 1990.
Petters, M. D. and Kreidenweis, S. M.: A single parameter representation of hygroscopic growth and cloud condensation nucleus activity, Atmos. Chem. Phys., 7, 1961–1971, doi:10.5194/acp-7-1961-2007, 2007.
Petzold, A., Kopp, C., and Niessner, R.: The dependence of the specific attenuation cross-section on black carbon mass fraction and particle size, Atmos. Environ., 31, 661–672, 1997.
Poppe, D., Wallasch, M., and Zimmermann, J.: The dependence of the concentration of OH on its precursors under moderately polluted conditions: a model study, J. Atmos. Chem., 16, 61–78, 1993.
Ritesh, G., Christina, H., Menas, K., and Si-Chee, T.: Influences of winter haze on fog/low cloud over the Indo-Gangetic plains, J. Geophys. Res., 112, D05207, doi:10.1029/2005JD007036, 2007.
Roberts, G. C. and Nenes, A.: A continuous-flow streamwise thermal-gradient CCN chamber for atmospheric measurements, Aerosol Sci. Tech., 39, 206–221, 2006.
Schichtel, B. A., Husar, R. B., Falke, S. R., and Wilson, W. E.: Haze trends over the United States, 1980–1995, Atmos. Environ., 35, 5205–5210, 2001.
Sun, Y. L., Zhuang, G. S., Wang, Y., Han, L. H., Guo, J. H., Dan, M., Zhang, W. J., Wang, Z. F., and Hao, Z. P.: The air-borne particulate pollution in Beijing-Concentration, composition, distribution and sources, Atmos. Environ., 38, 5991–6004, 2004.

ACPD
15, 32561–32605, 2015

Sun, Y. L., Zhuang, G. S., Tang, A. H., Wang, Y., and An, Z. S.: Chemical characteristics of $PM_{2.5}$ and PM_{10} in haze-fog episodes in Beijing, Environ. Sci. Technol., 40, 3148–3155, 2006.
Quinn, P. K. and Bates, T.: North American, Asian, and Indian haze: similar regional impacts on climate?, Geophys. Res. Lett., 30, 1555, doi:10.1029/2003GL016934, 2003.
Seinfeld, J. H. and Pandis, S. N.: Atmospheric Chemistry and Physics: from Air Pollution to Climate Change, 2nd edn., John Wiley & Sons, New York, USA, 57–58 and 381–383, 2006.
Tan, H. H., Duan, J. C., He, K. B., Ma. Y. L., Duan, F. K., Chen, Y., and Fu, J. M.: Chemical characteristics of $PM_{2.5}$ during a typical haze episode in Guangzhou, J. Environ. Sci., 21, 774–781, 2009.
Tang, I. N.: Chemical and size effects of hygroscopic aerosols on light scattering coefficients, J. Geophys. Res., 101, 19245–19250, 1996.
Tie, X. X., Wu, D., and Brasseur, G.: Lung cancer mortality and exposure to atmospheric aerosol particles in Guangzhou, China, Atmos. Environ., 43, 2375–2377, 2009.
Wang, Y., Zhuang, G. S., Zhang, X. Y., Huang, K., Xu, C., Tang, A. H., Chen, J. M., and An, Z. S.: The ion chemistry, seasonal cycle, and sources of $PM_{2.5}$ and TSP aerosol in Shanghai, Atmos. Environ., 40, 2935–2952, 2006a.
Wang, Y., Zhuang, G. S., Sun, Y. L., and An, Z. S.: The variation of characteristics and formation mechanisms of aerosols in dust, haze, and clear days in Beijing, Atmos. Environ., 40, 6579–6591, 2006b.
Weingartner, E., Saathoff, H., Schnaiter, M., Streit, N., Bitnar, B., and Baltensperger, U.: Absorption of light by soot particles: determination of the absorption coefficient by means of aethalometers, J. Aerosol Sci., 34, 1445–1463, 2003.
Woo, K. S., Chen, D. R., Pui, D. Y. H., and McMurry, P. H.: Measurements of Atlanta aerosol size distributions: observations of ultrafine particle events, Aerosol Sci. Tech., 34, 75–87, 2001.
Wu, D., Tie, X., Li, C., Ying, Z., Lau, A. K.-H., Huang, J., Deng, X., and Bi, X.: An extremely low visibility event over the Guangzhou region: a case study, Atmos. Environ., 39, 6568–6577, 2005.
Wu, D., Bi, X., Deng, X., Li, F., Tan, H., Liao, G., and Huang, J.: Effects of atmospheric haze on the deterioration of visibility over the Pearl River Delta, Acta Meteorol. Sin., 64, 510–517, 2006.
Xiao, F., Brajer, V., and Mead, R. W.: Blowing in the wind: the impact of China's Pearl River Delta on Hong Kong's air quality, Sci. Total Environ., 367, 96–111, 2006.

ACPD
15, 32561–32605, 2015

Xu, W. Y., Zhao, C. S., Ran, L., Deng, Z. Z., Liu, P. F., Ma, N., Lin, W. L., Xu, X. B., Yan, P., He, X., Yu, J., Liang, W. D., and Chen, L. L.: Characteristics of pollutants and their correlation to meteorological conditions at a suburban site in the North China Plain, Atmos. Chem. Phys., 11, 4353–4369, doi:10.5194/acp-11-4353-2011, 2011.

Yao, X. H., Chan, C. K., Fang, M., Cadle, S., Chan, T., Mulawa, P., He, K. B., and Ye, B. M.: The water-soluble ionic composition of $PM_{2.5}$ in Shanghai and Beijing, China, Atmos. Environ., 36, 4223–4234, 2002.

Ye, X. N., Ma, Z., Zhang, J. C., Du, H. H., Chen, J. M., Chen, H., Yang, X., Gao, W., and Geng, F. H.: Important role of ammonia on haze formation in Shanghai, Environ. Res. Lett., 6, 24019–24023, doi:10.1088/1748-9326/6/2/024019, 2011.

Yue, D. L., Hu, M., Zhang, R. J., Wu, Z. J., Su, H., Wang, Z. B., Peng, J. F., He, L. Y., Huang, X. F., Gong, Y. G., and Wiedensohler, A.: Potential contribution of new particle formation to cloud condensation nuclei in Beijing, Atmos. Environ., 45, 6070–6077, 2011.

Zhang, M., Wang, X. M., Chen, J. M., Cheng, T. T., Wang, T., Yang, X., Gong, Y. G., Geng, F. H., and Chen, C. H.: Physical characterization of aerosol particles during the Chinese New Year's firework events, Atmos. Environ., 44, 5191–5198, 2010.

Zhang, Q. C., Zhu, B., Su, J. F., and Wang, H. L.: Characteristcs of aerosol water-soluble inorganic ions in three types air-pollution incidents of Nanjing City, Environ. Sci., 33, 1944–1951, 2012 (in Chinese).

Zhao, P. S., Dong, F., He, D., Zhao, X. J., Zhang, X. L., Zhang, W. Z., Yao, Q., and Liu, H. Y.: Characteristics of concentrations and chemical compositions for $PM_{2.5}$ in the region of Beijing, Tianjin, and Hebei, China, Atmos. Chem. Phys., 13, 4631–4644, doi:10.5194/acp-13-4631-2013, 2013.

Zhao, X. J., Zhao, P. S., Xu, J., Meng, W., Pu, W. W., Dong, F., He, D., and Shi, Q. F.: Analysis of a winter regional haze event and its formation mechanism in the North China Plain, Atmos. Chem. Phys., 13, 5685–5696, doi:10.5194/acp-13-5685-2013, 2013.

ACPD
15, 32561–32605, 2015

Table 1. Effective hygroscopicity parameters (κ) and densities of the three category compositions.

Species	Data source	κ	Density ($g\,cm^{-3}$)
Sulfate & nitrate	$SO_4^{2-} + NO_3^- + NH_4^+$	0.6	1.7
Sodium chloride	$Cl^- + Na^+$	1	2.2
Insoluble compounds	Others	0	2.0

ACPD
15, 32561–32605, 2015

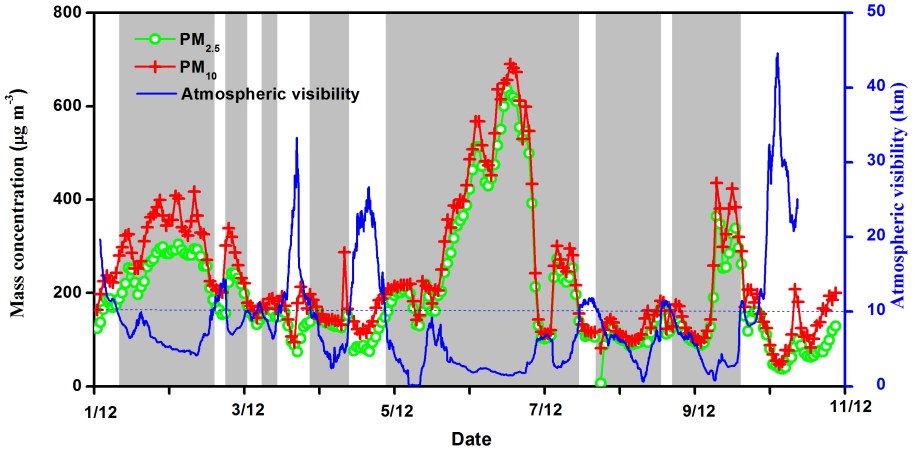

Figure 1. Temporal variations of $PM_{2.5}$, PM_{10} and atmospheric visibility (vis) measured in Shanghai from 1 to 10 December 2013. The dash line is vis at 10 km.

ACPD
15, 32561–32605, 2015

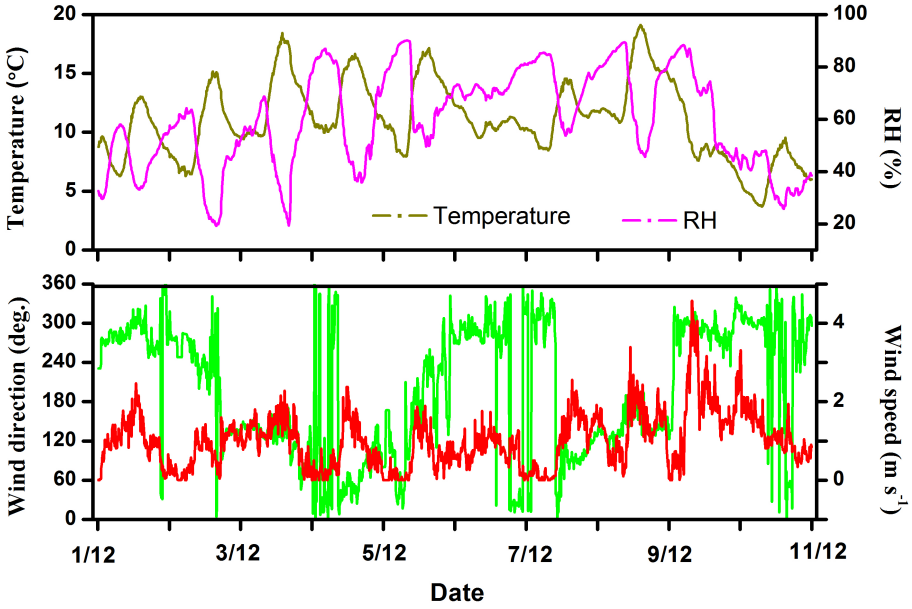

Figure 2. Temporal variations of meteorological parameters from 1 to 10 December 2013.

ACPD
15, 32561–32605, 2015

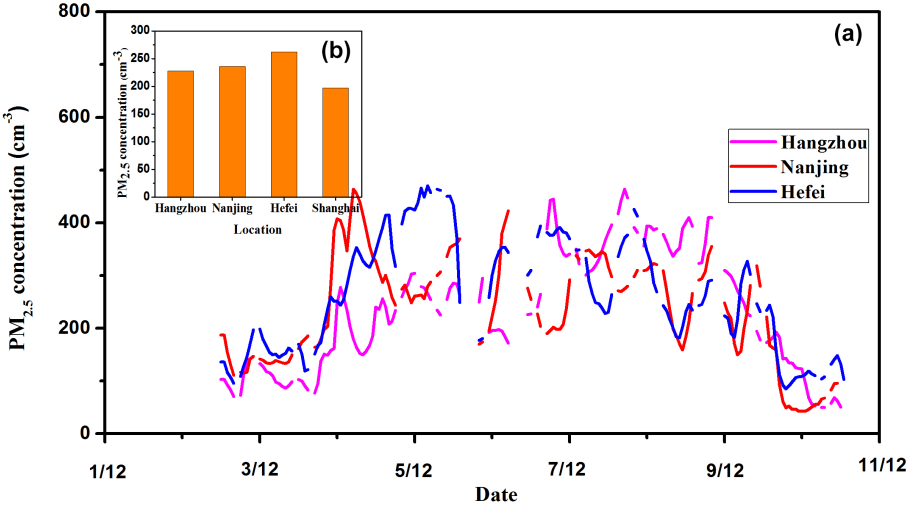

Figure 3. Temporal variations of $PM_{2.5}$ in Hangzhou, Nanjing and Hefei **(a)** and their mean concentrations **(b)** from 1 to 10 December 2013.

ACPD
15, 32561–32605, 2015

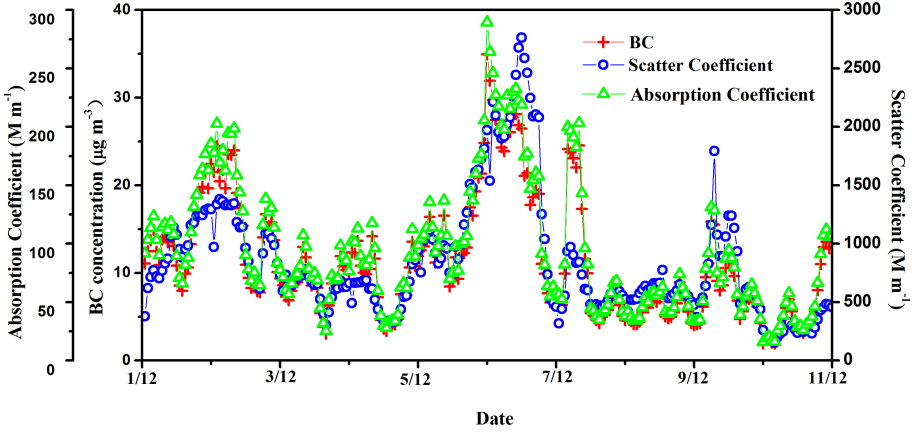

Figure 4. Temporal variations of black carbon (BC) concentration, aerosol scattering (Sc) and absorptive (Ab) coefficients from 1 to 10 December 2013.

ACPD
15, 32561–32605, 2015

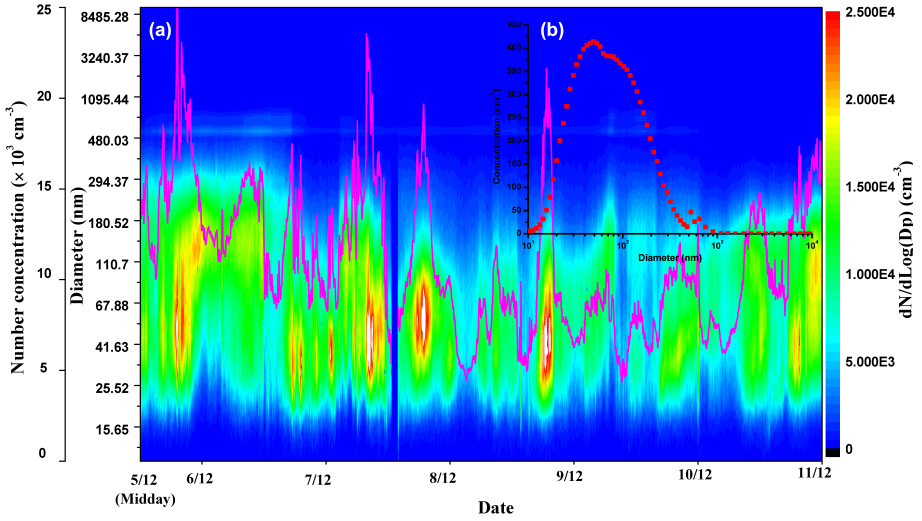

Figure 5. Time series of 4 min mean aerosol number size spectra and integrating number concentration (pink line, **a**) and averaged aerosol number size distribution **(b)** from 5 to 10 December 2013.

ACPD
15, 32561–32605, 2015

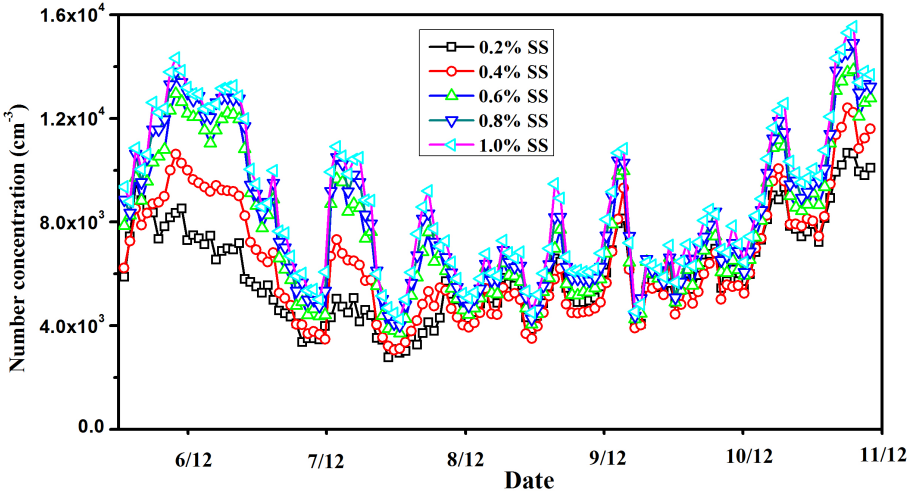

Figure 6. Time series of 1 h mean CCN concentration (N_{CCN}) at supersaturations (SS) of 0.2–1.0 % from 5 to 10 December.

ACPD
15, 32561–32605, 2015

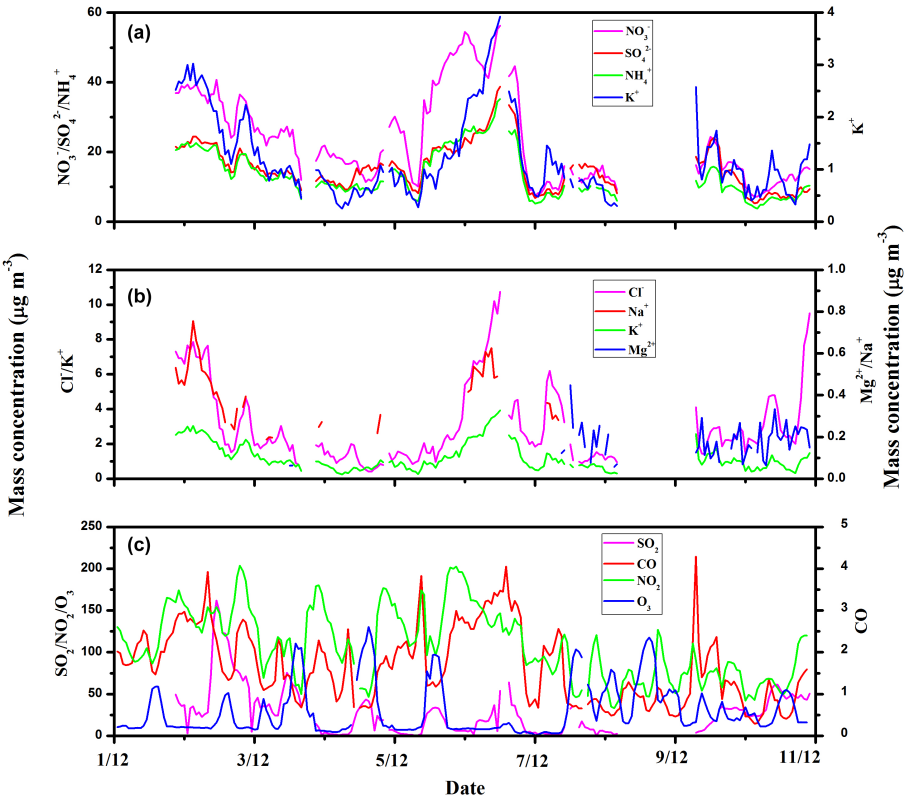

Figure 7. Temporal variations of chemical species in particles from 1 to 10 December 2013.

ACPD
15, 32561–32605, 2015

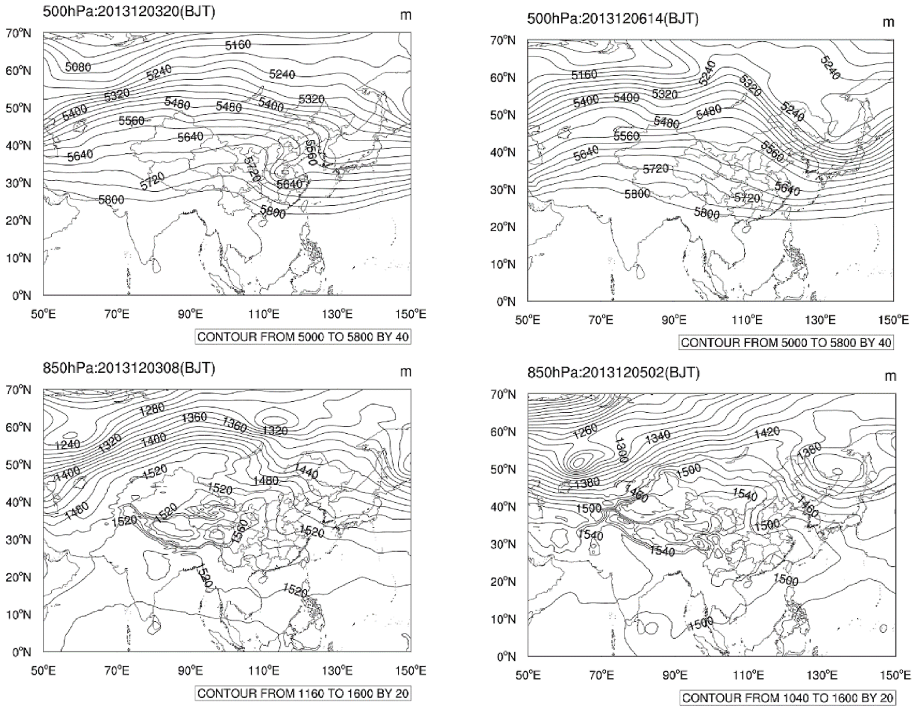

Figure 8. Atmospheric circulation situation at 500 and 850 hPa from 3 to 6 December 2013.

ACPD
15, 32561–32605, 2015

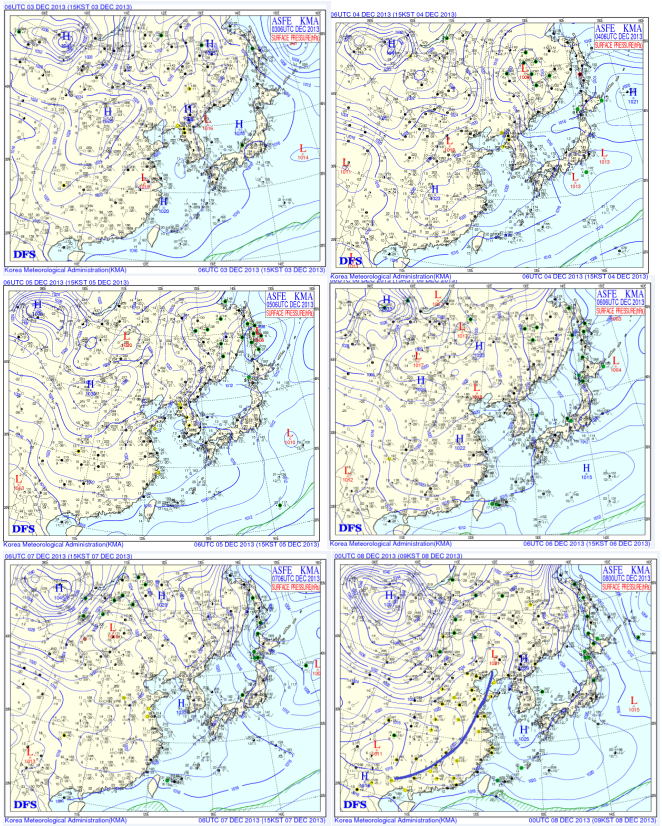

Figure 9. Surface weather maps at 06:00 (UTC) from 3 to 8 December 2013. The black star denotes the measurement site http://qixiangxinxifabupingtai.ejinqiao.com.

ACPD
15, 32561–32605, 2015

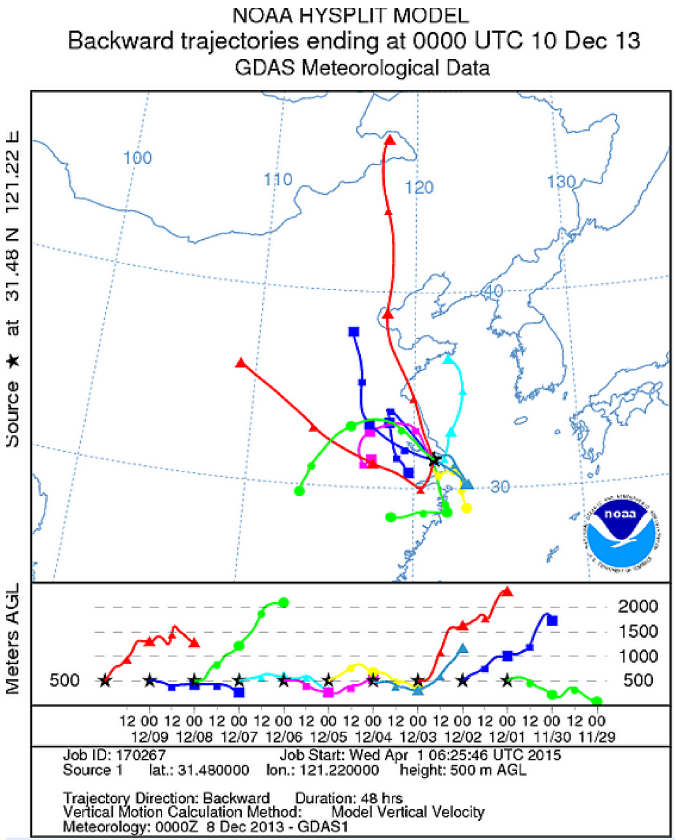

Figure 10. Air mass 48 h backward trajectories arriving at Shanghai from 1 to 10 December 2013 (500 m). A new trajectory is started at 0:00 (UTC) and calculated every 24 h.

ACPD
15, 32561–32605, 2015

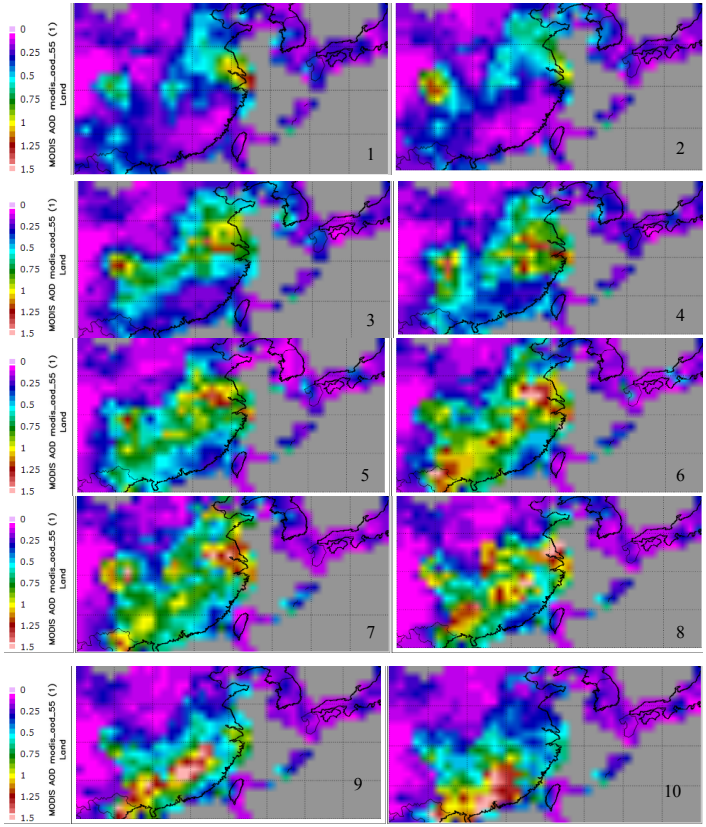

Figure 11. Aerosol optical depth (AOD) at 550 nm from MODIS over the YRD region at 06:00 (UTC) from 1 to 10 December 2013 (http://modis.gsfc.nasa.gov/).

ACPD
15, 32561–32605, 2015

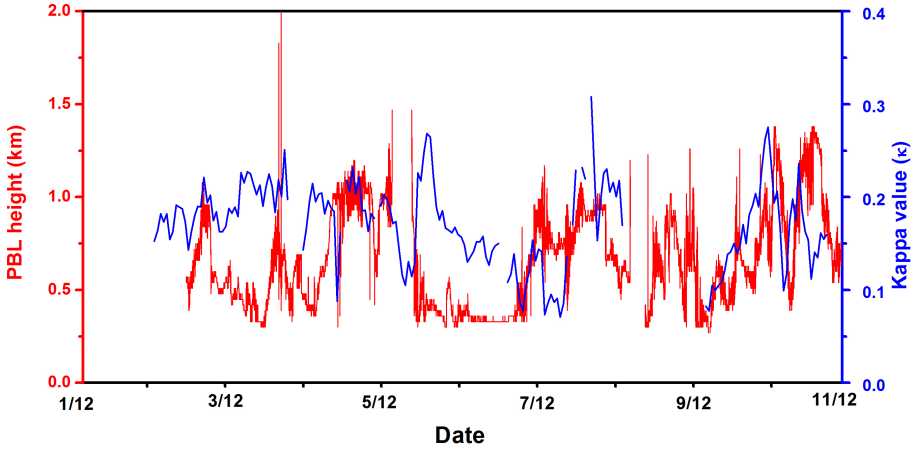

Figure 12. Time series of 1 h mean kappa value (i.e. κ) and 5 min mean PBL height from 1 to 10 December.

ACPD
15, 32561–32605, 2015

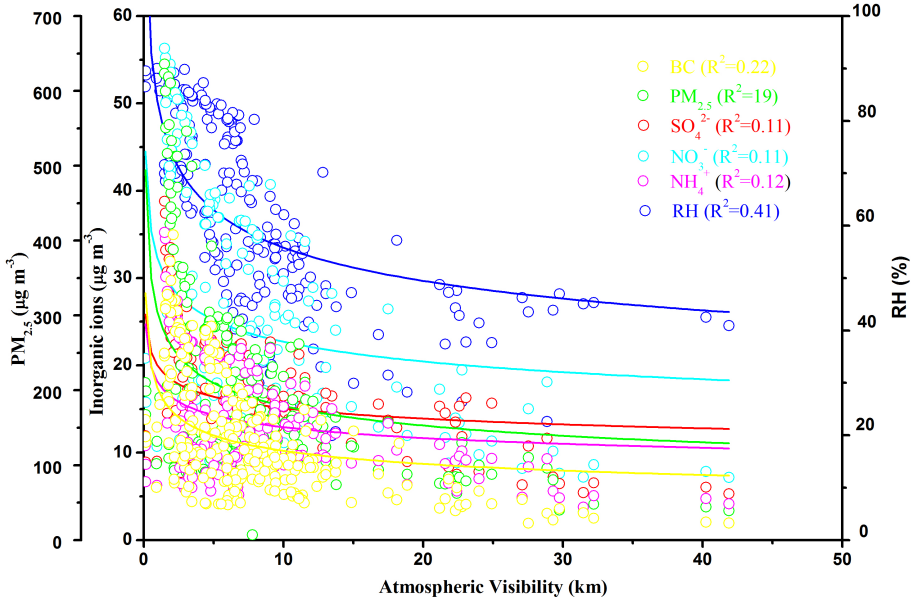

Figure 13. Scatter plots of RH, BC, $PM_{2.5}$ and inorganic ions in particles vs. atmospheric visibility.

ACPD
15, 32561–32605, 2015

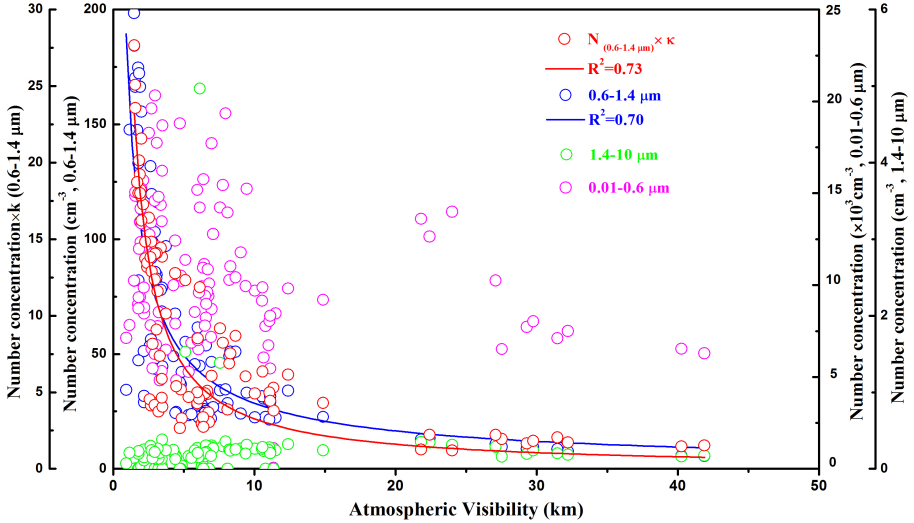

Figure 14. Scatter plots of aerosol number concentrations in ranges of 0.01–0.6, 0.6–1.4 and 1.4–10 μm, and aerosol number concentration (0.6–1.4 μm) multiplied by particle hygroscopcity (kappa value, κ) vs. atmospheric visibility.

ACPD
15, 32561–32605, 2015